




## Research Article

# Interaction of Screw Dislocation with Edge Interfacial Crack on Fine-Grained Piezoelectric Coating/Substrate

Shuaishuai Hu <sup>1</sup>, Jiansheng Liu,<sup>1</sup> Junlin Li <sup>2</sup>, and Xiufeng Xie <sup>2</sup>

<sup>1</sup>School of Materials Science and Engineering, Taiyuan University of Science and Technology, Taiyuan 030024, China

<sup>2</sup>School of Applied Science, Taiyuan University of Science and Technology, Taiyuan 030024, China

Correspondence should be addressed to Junlin Li; [lijunlin9762@163.com](mailto:lijunlin9762@163.com) and Xiufeng Xie; [xxf21@126.com](mailto:xxf21@126.com)

Received 28 February 2019; Revised 13 September 2019; Accepted 14 September 2019; Published 19 November 2019

Academic Editor: Jose M. Cabrera

Copyright © 2019 Shuaishuai Hu et al. This is an open access article distributed under the Creative Commons Attribution License, which permits unrestricted use, distribution, and reproduction in any medium, provided the original work is properly cited.

The interaction between micro- and macrocracks in a fine-grained piezoelectric coating/substrate under remote antiplane mechanical and in-plane electrical loadings was studied. The principle of superposition and a mapping function method was used to transform the fine-grained coating/substrate structure containing the screw dislocation and the edge interfacial crack into the right semi-infinite plane piezoelectric bimaterial with screw dislocation to simplify the problem. Furthermore, the electric field, displacement field, intensity factors, and image force of these two problems were established. In addition, numerical calculations were then given graphically to study the effects of the elastic modulus of the material, the size of the crack, the thickness of the coating, and the screw dislocation angle on the edge interface crack and dislocation.

## 1. Introduction

Piezoelectric materials have been widely applied to modern devices, such as sensors, actuators, and transducers, due to their intrinsic electromechanical coupling ability. At the same time, it is easy to affect the performance and strength of the devices and structures on a number of scales (micro and macro, e.g., dislocations and cracks) based on the characteristics of the piezoelectric material and the defects of the processing technology. Therefore, the defects of piezoelectric materials under mechanical and electrical loads have attracted wide attention [1–4]. Pak [5] derived the interaction energy for two different internal stress-field systems and utilized the standard method and a generalized path-independent integral to calculate the force on a piezoelectric screw dislocation subjected to external mechanical and electrical loads. Liu et al. [6] revealed the degree of influence of electromechanical coupling behavior on the image force on a screw dislocation. Jin and Fang [7] investigated the electroelastic coupling interaction between multiple screw dislocations that may be located either outside or inside the inclusion and a circular inclusion with an imperfect interface in a piezoelectric solid.

Wang and Xu [8] analytically discovered the contribution of surface piezoelectricity to the interaction between a piezoelectric screw dislocation and a finite crack in a hexagonal piezoelectric solid. Bagheri et al. [9] explored the problem of a screw dislocation located in a substrate imperfectly bonded to a coating, and the dislocation density was used to determine the field intensity factors. Zhang et al. [10] investigated the interaction between a screw dislocation and a circular nanoinhomogeneity with a semi-infinite wedge crack penetrating the interface, and the influence of elastic mismatch of materials, inhomogeneity size, interface stress, and wedge-crack opening angle was studied. Shen and Hung [11] examined the interaction between a screw dislocation and an oblique edge crack in a semi-infinite piezoelectric medium under remote antiplane mechanical and in-plane electrical loadings. Liu et al. [12] dealt with the influence of a Kelvin-type viscoelastic interface on the generation of screw dislocations near the interfacial blunt crack tip in light of a pair of concentrated loads via the integral transform and conformal mapping. Fan et al. [13, 14] investigated a curved interface crack between a circular inclusion and an infinite matrix and discussed the influence of the material properties and other geometric

parameters on the stress intensity factors, plastic zone size, and crack tip opening displacement. In another article considered, the elastic-plastic stress analysis on a matrix crack interacting with nearby circular inclusions in fiber-reinforced composites was considered, and with the aid of the distributed dislocation method, the effective stress intensity factor, PZS, and crack tip opening displacement were evaluated.

However, all of polycrystalline materials studied above composed of multidomain grains of size from several microns to tens of micrometers, and the sizes cannot meet the requirements of the present work. Reducing the particle size to the submicron level can improve the machinability of the material and the mechanical strength of the resulting device. In recent years, fine-grained piezoelectric materials have been used for cutting and grinding, and some high-frequency transducers, microbrakes, and thin buzzers have been fabricated in which the advantages of fine-grained piezoelectric materials have been proved. In these works, the effects of grain size on the phase structure, density, and the dielectric and piezoelectric properties were investigated [15–17]. However, the mechanical properties of fine-grained piezoelectric materials with defects were not studied, and fine-grained piezoelectric materials are required to be in the form of coatings, especially in some special applications.

In the work described in this paper, the fine-grained piezoelectric coating/substrate mechanical model was established, in which the interaction between the screw dislocation and the edge interfacial crack was presented. The superposition principle and the mapping function method were utilized to transform the coating/substrate structure into the right semi-infinite plane piezoelectric bimaterial structure, and the analytical expressions of the image force and intensity factor for the mechanical model were obtained. Furthermore, the influence of various material parameters on image force and intensity factor was analyzed by numerical calculation.

## 2. Problem Formulation

As shown in Figure 1, the coating and the substrate are bonded together by plasma spraying, while the edge crack with a length of  $a$  is along the interface between the coating and substrate. The coating/substrate structure is considered as a strip with limited thickness along  $Y$  axis and infinite length along  $X$  axis. The thicknesses of the coating and the substrate are  $h_1$  and  $h_2$ , respectively. Assume that the poling direction  $Z$  normal to the  $X - Y$  plane and the screw dislocation  $\mathbf{b} = [b_z, b_\phi]$  with dislocation line parallel to the poling direction are situated at  $z_0$  in fine-grained piezoelectric coating, in which  $b_z$  and  $b_\phi$  are the classical elastic displacement jump and the electric potential jump, respectively. The coating/substrate structure are linearly elastic, homogeneous, isotropic, and piezoelectric. Their physical properties are defined by the elastic constants ( $c_{44}$ ), the piezoelectric constants ( $e_{15}$ ), and the dielectric constants ( $\epsilon_{11}$ ).

The piezoelectric boundary value problem is only considered in the case of out of plane displacement  $w$  and in-plane electric potential  $\phi$  field such that

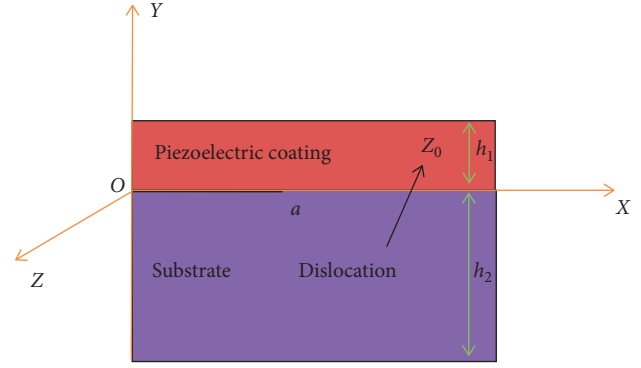


FIGURE 1: The fine-grained piezoelectric coating/substrate structure.

$$\begin{aligned} U &= V = 0, \\ W &= W(x, y), \\ \Phi &= \Phi(x, y). \end{aligned} \quad (1)$$

In this case, the constitutive equations become

$$\sigma_{xz} = c_{44}^{(n)} \frac{\partial W}{\partial x} + e_{15}^{(n)} \frac{\partial \Phi}{\partial x}, \quad (2)$$

$$D_x = e_{15}^{(n)} \frac{\partial W}{\partial x} - \epsilon_{11}^{(n)} \frac{\partial \Phi}{\partial x}, \quad (3)$$

$$\sigma_{yz} = c_{44}^{(n)} \frac{\partial W}{\partial y} + e_{15}^{(n)} \frac{\partial \Phi}{\partial y}, \quad (4)$$

$$D_y = e_{15}^{(n)} \frac{\partial W}{\partial y} - \epsilon_{11}^{(n)} \frac{\partial \Phi}{\partial y}. \quad (5)$$

In equations (2)–(5),  $\sigma_{mz}$  is the stress tensor,  $D_m$  ( $m = x, y$ ) is the electric displacement vector,  $c_{44}^{(n)}$  is the elastic modulus measured at constant electric field,  $e_{15}^{(n)}$  and  $\epsilon_{11}^{(n)}$  are the piezoelectric and dielectric constants, and the superscript  $n$  ( $n = 1, 2$ ) stands for the upper and lower piezoelectric materials, respectively.

The electric field can be given by the following form:

$$\begin{aligned} E_x &= -\frac{\partial \Phi}{\partial x}, \\ E_y &= -\frac{\partial \Phi}{\partial y}. \end{aligned} \quad (6)$$

According to [1], the governing equations are simplified to

$$c_{44}^{(n)} \nabla^2 W + e_{15}^{(n)} \nabla^2 \Phi = 0, \quad (7)$$

$$e_{15}^{(n)} \nabla^2 W - \epsilon_{11}^{(n)} \nabla^2 \Phi = 0, \quad n = 1, 2. \quad (8)$$

The governing equations (7) and (8) can be reduced to the more compact form:

$$\begin{aligned} \nabla^2 W &= 0, \\ \nabla^2 \Phi &= 0, \end{aligned} \quad (9)$$

where  $\nabla^2$  is the two-dimensional Laplacian operator.

For simplicity, we define the displacement vector  $\mathbf{u} = [W, \Phi]^T$  and the stress vector  $\mathbf{t}_m = [\sigma_{mz}, D_m]^T$ , where the T represents the transposing of the matrix.

Consequently equations (2)–(5) and (9) can be made in the forms

$$\begin{aligned} \nabla^2 \mathbf{u} &= 0, \\ \mathbf{t}_m &= \mathbf{L}^{(n)} \frac{\partial \mathbf{u}}{\partial m}, \quad m = x, y, \end{aligned} \quad (10)$$

where

$$\mathbf{L}^{(n)} = \begin{bmatrix} c_{44}^{(n)} & e_{15}^{(n)} \\ e_{15}^{(n)} & -\varepsilon_{11}^{(n)} \end{bmatrix}, \quad n = 1, 2. \quad (11)$$

According to the theory of complex functions, the general solution to equation (10) takes the following form:

$$\mathbf{u} = \text{Imf}(z), \quad (12)$$

in which  $\mathbf{f}(z) = [f_{(1)}(z), f_{(2)}(z)]^T$  is an analytical function vector of the complex variable  $z = x + iy$ , where Im stands for the imaginary part and  $i = \sqrt{-1}$ . Substituting equations (11) into (10), the expressions of stress and electric displacement are obtained:

$$\mathbf{t}_y + i\mathbf{t}_x = \mathbf{L}^{(n)} \mathbf{f}'(z). \quad (13)$$

By using the principle of superposition, the problem can be regarded as the sum of a homogeneous problem without crack and a nonhomogeneous problem of edge interface crack and screw dislocation.

The boundary conditions can be written as

$$\begin{aligned} \sigma_{yz}(x, h_1) &= \sigma_{yz}(x, -h_2) = 0, \quad 0 \leq x < +\infty, \\ D_y(x, h_1) &= D_y(x, -h_2) = 0, \quad 0 \leq x < +\infty, \\ \sigma_{yz}(x, 0^+) &= \sigma_{yz}(x, 0^-), \quad |x| > a, \\ D_y(x, 0^+) &= D_y(x, 0^-), \quad |x| > a, \\ W(x, 0^+) &= W(x, 0^-), \quad |x| > a, \\ \Phi(x, 0^+) &= \Phi(x, 0^-), \quad |x| > a, \\ \sigma_{yz}(x, 0^+) &= \sigma_{yz}(x, 0^-) = 0, \quad |x| > a, \\ D_y(x, 0^+) &= D_y(x, 0^-) = 0, \quad |x| > a, \end{aligned} \quad (14)$$

$$\oint_{\Omega} d\mathbf{u} = b,$$

$$\oint_{\Omega} t_y dx - t_x dy = 0,$$

where  $\Omega$  stands for the any closed curve around the dislocation  $z_0$ .

### 3. Solution to the Problem

**3.1. Transformation of Problem.** According to the above discussion, we only need to determine the analytic function of  $\mathbf{f}(z)$ . By using the principle of superposition, the problem stated in the previous section can be expressed in Figure 2.

In order to obtain the solution of the problem shown in Figure 2, two mapping functions were used to simplify the problem:

$$\zeta = -i \left[ \frac{1 + ie^{\pi i / (h_1 + h_2)} (2 - ((h_1 - h_2)/2)i)}{1 - ie^{\pi i / (h_1 + h_2)} (2 - ((h_1 - h_2)/2)i)} \right]^2, \quad (15)$$

$$\xi = \sqrt{\zeta^2 - a^2}, \quad (16)$$

which transforms the regions occupied by piezoelectric coating and dislocation in the  $z$ -plane into the right semi-infinite of the  $\xi$  plane and dislocation point changed from  $z_0$  to  $\xi_0$ , as follows, in Figures 3(c) and 3(d), where  $\eta$  and  $\varsigma$  are the real and imaginary parts of the corresponding complex variables, respectively. Equations (15) and (16) are explained in Figures 4 and 5 in Appendix.

**3.2. Screw Dislocation of the Right Semi-Infinite Piezoelectric Composite Medium.** From the above statement, it can be noted that what we only need is to get the screw dislocation in the right semi-infinite piezoelectric composite medium.

According to the boundary conditions, assume that the unknown functions  $f_{(1)}(z)$  and  $f_{(2)}(z)$  have the following forms in the mapped plane [6]:

$$f_{(1)}(z) = f_{(1)}^s(z) + f_{(1)}^p(z), \quad (17)$$

$$f_{(2)}(z) = f_{(2)}^p(z), \quad (18)$$

$$f_{(1)}^p(z) = \mathbf{A} [\ln(z - z_0) - \ln(z + \bar{z}_0)], \quad (19)$$

$$f_{(1)}^s(z) = \mathbf{G} \cdot \overline{f_{(1)}^p(z)}, \quad (20)$$

$$\begin{aligned} f_{(2)}^p(z) &= (\mathbf{I} - \mathbf{G}) \cdot f_{(1)}^p(z), \\ \mathbf{A} &= \frac{\mathbf{b}}{2\pi}, \end{aligned} \quad (21)$$

where  $f_{(1)}^s(z)$  represents the function associated with the unperturbed fields which are related to the solution of the corresponding homogeneous media subject to a piezoelectric screw dislocation and holomorphic in the entire domain except at  $z_0$ ,  $f_{(1)}^p(z)$ , and  $f_{(2)}^p(z)$  are the holomorphic function corresponding to the perturbed fields in the

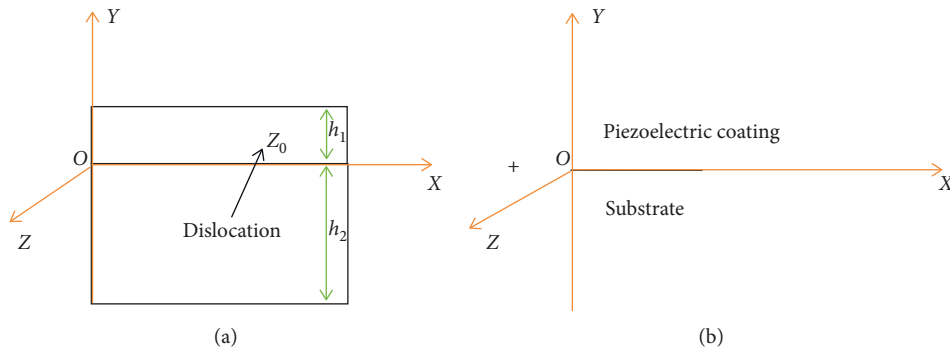


FIGURE 2: Superposition scheme: (a) a screw dislocation near interface of the fine-grained piezoelectric coating/substrate; (b) an edge interfacial crack of the half semi-infinite plane piezoelectric bimaterials.

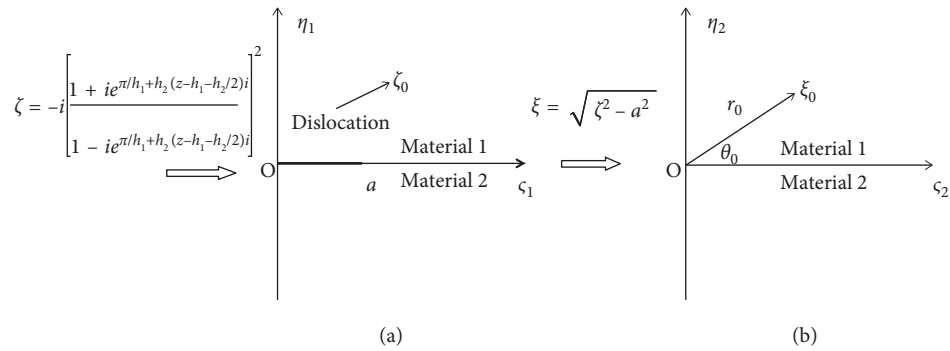


FIGURE 3: A screw dislocation interaction with an edge interfacial crack in the right semi-infinite plane piezoelectric bimaterials.

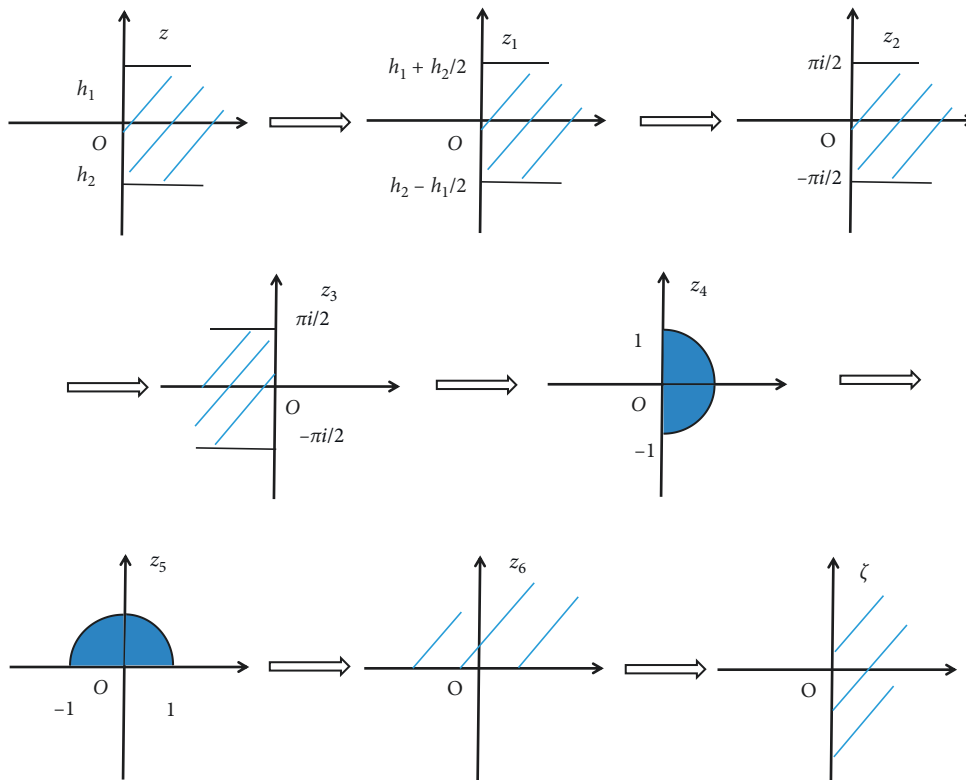


FIGURE 4

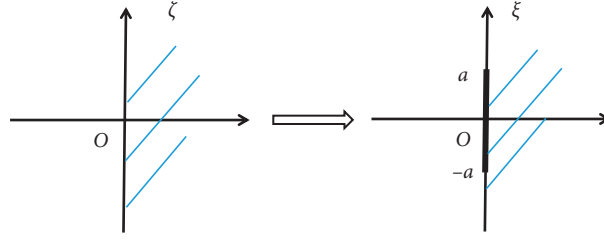


FIGURE 5

domain where the coating and substrate are located, the overbar denotes the complex conjugate, and  $\mathbf{I}$  is a  $2 \times 2$  unit matrix. The matrix  $\mathbf{G}$  is

$$\mathbf{G} = (\mathbf{L}^{(1)} + \mathbf{L}^{(2)})^{-1} (\mathbf{L}^{(2)} - \mathbf{L}^{(1)}). \quad (22)$$

Substituting equation (19)–(20) into equations (17) and (18), the functions  $f_{(1)}(z)$  and  $f_{(2)}(z)$  in the  $z$ -plane can be written as

$$f_{(1)}(z) = \frac{\mathbf{b}}{2\pi} [\ln(z - z_0) - \ln(z + \bar{z}_0)] + \mathbf{G} [\ln(z - \bar{z}_0) - \ln(z + z_0)], \quad (23)$$

$$f_{(2)}(z) = \frac{\mathbf{b}}{2\pi} (\mathbf{I} - \mathbf{G}) [\ln(z - z_0) - \ln(z + \bar{z}_0)]. \quad (24)$$

By equation (13), the stresses and electric displacements can be obtained.

#### 4. Image Force and Intensity Factor

**4.1. Image Force on a Screw Dislocation.** As shown in Figures 3(c) and 3(d), in order to get the image force of the problem, in equations (23) and (24), use  $\xi$  instead of  $z$ . We got

$$f_{(1)}(\xi) = \frac{\mathbf{b}}{2\pi} \{ [\ln(\xi - \xi_0) - \ln(\xi + \bar{\xi}_0)] + \mathbf{G} [\ln(\xi - \bar{\xi}_0) - \ln(\xi + \xi_0)] \}, \quad (25)$$

$$f_{(2)}(\xi) = \frac{\mathbf{b}}{2\pi} (\mathbf{I} - \mathbf{G}) [\ln(\xi - \xi_0) - \ln(\xi + \bar{\xi}_0)]. \quad (26)$$

Substituting (16) into equations (25) and (26), we got

$$f_{(1)}(\zeta) = \frac{\mathbf{b}}{2\pi} \left\{ \left[ \ln\left(\sqrt{\zeta^2 - a^2} - \sqrt{\zeta_0^2 - a^2}\right) - \ln\left(\sqrt{\zeta^2 - a^2} + \sqrt{\zeta_0^2 - a^2}\right) \right] + \mathbf{G} \left[ \ln\left(\sqrt{\zeta^2 - a^2} - \sqrt{\zeta_0^2 - a^2}\right) - \ln\left(\sqrt{\zeta^2 - a^2} + \sqrt{\zeta_0^2 - a^2}\right) \right] \right\}, \quad (27)$$

$$f_{(2)}(\zeta) = \frac{\mathbf{b}}{2\pi} (\mathbf{I} - \mathbf{G}) \left[ \ln\left(\sqrt{\zeta^2 - a^2} - \sqrt{\zeta_0^2 - a^2}\right) - \ln\left(\sqrt{\zeta^2 - a^2} + \sqrt{\zeta_0^2 - a^2}\right) \right]. \quad (28)$$

Take the derivative of equations (27) and (28):

$$f'_{(1)}(\zeta) = \frac{\mathbf{b}}{2\pi} \frac{\zeta}{\sqrt{\zeta^2 - a^2}} (X_1 - \mathbf{G}Y_1), \quad (29)$$

$$f'_{(2)}(\zeta) = \frac{\mathbf{b}}{2\pi} (\mathbf{I} - \mathbf{G}) \frac{\zeta}{\sqrt{\zeta^2 - a^2}} X_1,$$

where

$$X_1 = \frac{1}{\sqrt{\zeta^2 - a^2} - \sqrt{\zeta_0^2 - a^2}} - \frac{1}{\sqrt{\zeta^2 - a^2} + \sqrt{\zeta_0^2 - a^2}}, \quad (30)$$

$$Y_1 = \frac{1}{\sqrt{\zeta^2 - a^2} - \sqrt{\zeta_0^2 - a^2}} - \frac{1}{\sqrt{\zeta^2 - a^2} + \sqrt{\zeta_0^2 - a^2}}.$$

According to the generalized Peach-Koehler formula derived in [5] for piezoelectric materials, we have

$$\begin{aligned} F_x &= \mathbf{b}^T t_{yp}^{(1)}(\zeta_0), \\ F_y &= -\mathbf{b}^T t_{xp}^{(1)}(\zeta_0), \end{aligned} \quad (31)$$

where  $t_{mp}^{(1)}(\zeta_0)$  ( $m = x, y$ ) is the perturbed stresses and electric displacements at  $z_0$ .

By equation (13), the following equation can be obtained:

$$F_x - iF_y = \mathbf{b}^T [t_{yp}^{(1)}(\zeta_0) + it_{xp}^{(1)}(\zeta_0)] = \mathbf{b}^T \mathbf{L}^{(1)} [f'_{(1)} - f'_{(1\infty)}], \quad (32)$$

with

$$f'_{(1\infty)} = \frac{\mathbf{b}}{2\pi} \ln \left( \sqrt{\zeta^2 - a^2} - \sqrt{\zeta_0^2 - a^2} \right). \quad (33)$$

From equations (32), the image force of the right semi-infinite plane piezoelectric bimaterial can be obtained:

$$F_x - iF_y = \frac{\mathbf{b}\mathbf{b}^T}{2\pi} \mathbf{L}^{(1)} \left( -\frac{1}{\sqrt{\zeta_0^2 - a^2} + \sqrt{\zeta_0^2 - a^2}} - \mathbf{G}Y_1 \right) \cdot \frac{\zeta_0}{\sqrt{\zeta_0^2 - a^2}}, \quad (34)$$

$$F_x - iF_y = \frac{\mathbf{b}\mathbf{b}^T}{2\pi} \left[ \frac{(1 - c_{12})(1 + c_{44}^{(1)}v)}{2c_{12} + c_{44}^{(1)}v(1 + c_{12})} Y_1 - (1 - c_{12}) \frac{\sqrt{\zeta_0^2 - a^2} + \sqrt{\zeta_0^2 - a^2}}{\zeta_0^2 - \zeta_0'^2} \right] \cdot \frac{\zeta_0}{\sqrt{\zeta_0^2 - a^2}}, \quad (35)$$

$$\begin{aligned} c_{12} &= \frac{c_{44}^{(1)}}{c_{44}^{(2)}}, \\ v &= \frac{\varepsilon_{11}^{(1)}}{e_{15}^{(1)2}}. \end{aligned} \quad (36)$$

Here, we only need to get the real and imaginary parts of equation (34), and then the image force of the screw dislocation as shown in Figure 2(b) can be obtained.

Substituting equation (15) into equations (27) and (28), we got

$$\begin{aligned} f_{(1)}(z) &= \frac{\mathbf{b}}{2\pi} \left\{ \ln \left( \sqrt{\frac{1 + ie^{\pi/(h_1+h_2)}(z - ((h_1-h_2)/2)i)}{1 - ie^{\pi/(h_1+h_2)}(z - ((h_1-h_2)/2)i)}}^4 - a^2} - \sqrt{\frac{1 + ie^{\pi/(h_1+h_2)}(z_0 - ((h_1-h_2)/2)i)}{1 - ie^{\pi/(h_1+h_2)}(z_0 - ((h_1-h_2)/2)i)}}^4 - a^2} \right) \right. \\ &\quad - \ln \left( \sqrt{\frac{1 + ie^{\pi/(h_1+h_2)}(z - ((h_1-h_2)/2)i)}{1 - ie^{\pi/(h_1+h_2)}(z - ((h_1-h_2)/2)i)}}^4 - a^2} + \sqrt{\frac{1 + ie^{\pi/(h_1+h_2)}(\bar{z}_0 - ((h_1-h_2)/2)i)}{1 - ie^{\pi/(h_1+h_2)}(\bar{z}_0 - ((h_1-h_2)/2)i)}}^4 - a^2} \right) \\ &\quad + G \left[ \ln \left( \sqrt{\frac{1 + ie^{\pi/(h_1+h_2)}(z - ((h_1-h_2)/2)i)}{1 - ie^{\pi/(h_1+h_2)}(z - ((h_1-h_2)/2)i)}}^4 - a^2} - \sqrt{\frac{1 + ie^{\pi/(h_1+h_2)}(\bar{z}_0 - ((h_1-h_2)/2)i)}{1 - ie^{\pi/(h_1+h_2)}(\bar{z}_0 - ((h_1-h_2)/2)i)}}^4 - a^2} \right) \right. \\ &\quad \left. - \ln \left( \sqrt{\frac{1 + ie^{\pi/(h_1+h_2)}(z - ((h_1-h_2)/2)i)}{1 - ie^{\pi/(h_1+h_2)}(z - ((h_1-h_2)/2)i)}}^4 - a^2} + \sqrt{\frac{1 + ie^{\pi/(h_1+h_2)}(z_0 - ((h_1-h_2)/2)i)}{1 - ie^{\pi/(h_1+h_2)}(z_0 - ((h_1-h_2)/2)i)}}^4 - a^2} \right) \right] \left. \right\}, \end{aligned} \quad (37)$$

$$f_{(2)}(z) = \frac{\mathbf{b}}{2\pi} (\mathbf{I} - \mathbf{G}) \left[ \ln \left( \sqrt{\left[ \frac{1 + ie^{\pi/(h_1+h_2)}(z - ((h_1-h_2)/2)i}{1 - ie^{\pi/(h_1+h_2)}(z - ((h_1-h_2)/2)i)} \right]^4 - a^2} - \sqrt{\left[ \frac{1 + ie^{\pi/(h_1+h_2)}(z_0 - ((h_1-h_2)/2)i}{1 - ie^{\pi/(h_1+h_2)}(z_0 - ((h_1-h_2)/2)i)} \right]^4 - a^2} \right) \right. \\ \left. - \ln \left( \sqrt{\left[ \frac{1 + ie^{\pi/(h_1+h_2)}(z - ((h_1-h_2)/2)i}{1 - ie^{\pi/(h_1+h_2)}(z - ((h_1-h_2)/2)i)} \right]^4 - a^2} + \sqrt{\left[ \frac{1 + ie^{\pi/(h_1+h_2)}(\bar{z}_0 - ((h_1-h_2)/2)i}{1 - ie^{\pi/(h_1+h_2)}(\bar{z}_0 - ((h_1-h_2)/2)i)} \right]^4 - a^2} \right) \right]. \quad (38)$$

Take the derivative of equations (37) and (38):

$$f'_{(1)}(z) = - \frac{2\mathbf{b}e^{\pi/(h_1+h_2)}(z - ((h_1-h_2)/2)i}{(h_1 + h_2)(1 - ie^{\pi/(h_1+h_2)}(z - ((h_1-h_2)/2)i))^2} [(M_{11} - N_{11}) + \mathbf{G}(M_{12} - N_{12})] \cdot P_1, \\ f'_{(2)}(z) = - \frac{2\mathbf{b}e^{\pi/(h_1+h_2)}(z - ((h_1-h_2)/2)i}{(h_1 + h_2)(1 - ie^{\pi/(h_1+h_2)}(z - ((h_1-h_2)/2)i))^2} (\mathbf{I} - \mathbf{G})(M_{11} - N_{11}) \cdot P_1, \quad (39)$$

where

$$M_{11} = \frac{1}{\sqrt{\left[ \frac{1 + ie^{\pi/(h_1+h_2)}(z - ((h_1-h_2)/2)i}{1 - ie^{\pi/(h_1+h_2)}(z - ((h_1-h_2)/2)i)} \right]^4 - a^2} - \sqrt{\left[ \frac{1 + ie^{\pi/(h_1+h_2)}(z_0 - ((h_1-h_2)/2)i}{1 - ie^{\pi/(h_1+h_2)}(z_0 - ((h_1-h_2)/2)i)} \right]^4 - a^2}}, \\ N_{11} = \frac{1}{\sqrt{\left[ \frac{1 + ie^{\pi/(h_1+h_2)}(z - ((h_1-h_2)/2)i}{1 - ie^{\pi/(h_1+h_2)}(z - ((h_1-h_2)/2)i)} \right]^4 - a^2} + \sqrt{\left[ \frac{1 + ie^{\pi/(h_1+h_2)}(\bar{z}_0 - ((h_1-h_2)/2)i}{1 - ie^{\pi/(h_1+h_2)}(\bar{z}_0 - ((h_1-h_2)/2)i)} \right]^4 - a^2}}, \\ M_{12} = \frac{1}{\sqrt{\left[ \frac{1 + ie^{\pi/(h_1+h_2)}(z - ((h_1-h_2)/2)i}{1 - ie^{\pi/(h_1+h_2)}(z - ((h_1-h_2)/2)i)} \right]^4 - a^2} - \sqrt{\left[ \frac{1 + ie^{\pi/(h_1+h_2)}(\bar{z}_0 - ((h_1-h_2)/2)i}{1 - ie^{\pi/(h_1+h_2)}(\bar{z}_0 - ((h_1-h_2)/2)i)} \right]^4 - a^2}}, \\ N_{12} = \frac{1}{\sqrt{\left[ \frac{1 + ie^{\pi/(h_1+h_2)}(z - ((h_1-h_2)/2)i}{1 - ie^{\pi/(h_1+h_2)}(z - ((h_1-h_2)/2)i)} \right]^4 - a^2} + \sqrt{\left[ \frac{1 + ie^{\pi/(h_1+h_2)}(z_0 - ((h_1-h_2)/2)i}{1 - ie^{\pi/(h_1+h_2)}(z_0 - ((h_1-h_2)/2)i)} \right]^4 - a^2}}, \\ P_1 = \frac{1}{\sqrt{\left[ \frac{1 + ie^{\pi/(h_1+h_2)}(z - ((h_1-h_2)/2)i}{1 - ie^{\pi/(h_1+h_2)}(z - ((h_1-h_2)/2)i)} \right]^4 - a^2}} \cdot \left[ \frac{1 + ie^{\pi/(h_1+h_2)}(z - ((h_1-h_2)/2)i}{1 - ie^{\pi/(h_1+h_2)}(z - ((h_1-h_2)/2)i)} \right]^3. \quad (40)$$

From the previous discussion, the image force of the fine-grained piezoelectric coating/substrate can be expressed as

$$F_x - iF_y = - \frac{2\mathbf{L}^{(1)}\mathbf{G} \cdot e^{\pi/(h_1+h_2)}(z_0 - ((h_1-h_2)/2)i)\mathbf{b}\mathbf{b}^T}{(h_1 + h_2)(1 - ie^{\pi/(h_1+h_2)}(z_0 - ((h_1-h_2)/2)i))^2} [-N_{21} + \mathbf{G}(M_{22} - N_{22})] \cdot P_2, \\ F_x - iF_y = - \frac{2e^{\pi/(h_1+h_2)}(z_0 - ((h_1-h_2)/2)i)\mathbf{b}\mathbf{b}^T}{(h_1 + h_2)(1 - ie^{\pi/(h_1+h_2)}(z_0 - ((h_1-h_2)/2)i))^2} \left[ \frac{(1 - c_{12})(1 + c_{44}^{(1)}\nu)}{2c_{12} + c_{44}^{(1)}\nu(1 + c_{12})} \cdot (M_{22} - N_{22}) - (1 - c_{12})N_{21} \right] \cdot P_2, \quad (41)$$

where

$$c_{12} = \frac{c_{44}^{(1)}}{c_{44}^{(2)}},$$

$$v = \frac{\varepsilon_{11}^{(1)}}{e_{15}^{(1)2}},$$

$$N_{21} = \frac{1}{\sqrt{\left[1 + ie^{\pi i} (h_1+h_2) (z_0-(h_1-h_2)/2)i / 1 - ie^{\pi i} (h_1+h_2) (z_0-(h_1-h_2)/2)i\right]^4 - a^2} + \sqrt{\left[1 + ie^{\pi i} (h_1+h_2) (\bar{z}_0-(h_1-h_2)/2)i / (1 - ie^{\pi i} (h_1+h_2) (\bar{z}_0-(h_1-h_2)/2)i)\right]^4 - a^2}},$$

$$M_{22} = \frac{1}{\sqrt{\left[1 + ie^{\pi i} (h_1+h_2) (z_0-(h_1-h_2)/2)i / (1 - ie^{\pi i} (h_1+h_2) (z_0-(h_1-h_2)/2)i)\right]^4 - a^2} - \sqrt{\left[1 + ie^{\pi i} (h_1+h_2) (\bar{z}_0-(h_1-h_2)/2)i / (1 - ie^{\pi i} (h_1+h_2) (\bar{z}_0-(h_1-h_2)/2)i)\right]^4 - a^2}},$$

$$N_{22} = \frac{1}{\sqrt{\left[1 + ie^{\pi i} (h_1+h_2) (z_0-(h_1-h_2)/2)i / (1 - ie^{\pi i} (h_1+h_2) (z_0-(h_1-h_2)/2)i)\right]^4 - a^2} + \sqrt{\left[1 + ie^{\pi i} (h_1+h_2) (\bar{z}_0-(h_1-h_2)/2)i / (1 - ie^{\pi i} (h_1+h_2) (\bar{z}_0-(h_1-h_2)/2)i)\right]^4 - a^2}},$$

$$P_2 = \frac{1}{\sqrt{\left[1 + ie^{\pi i} (h_1+h_2) (z_0-(h_1-h_2)/2)i / (1 - ie^{\pi i} (h_1+h_2) (z_0-(h_1-h_2)/2)i)\right]^4 - a^2}} \cdot \frac{\left[1 + ie^{\pi i} (h_1+h_2) (z_0-(h_1-h_2)/2)i\right]^3}{\left[1 - ie^{\pi i} (h_1+h_2) (z_0-(h_1-h_2)/2)i\right]^4}. \quad (42)$$

**4.2. Intensity Factors.** In studying the interaction between dislocation and crack, the intensity factor can be used to analyze the shielding or antishielding effect of dislocation on cracks. In this section, our attention will focus on the electro-elastic fields near the tip of the edge crack where local electro-elastic field intensification usually occurs. For the antiplane problem of the piezoelectric materials, the intensity factors are defined by

$$\mathbf{K} = [k_\sigma, k_D]^T = \lim_{r \rightarrow 0} \sqrt{2\pi r} \mathbf{t}_y(r, 0), \quad (43)$$

where  $k_\sigma$  is the classical SIF,  $k_D$  is the EDIF, and  $\mathbf{t}_y = [\sigma_{yz}, D_y]$ . According to the boundary continuity conditions,  $\mathbf{t}_y(r, 0)$  in equation (43) can be replaced by  $\mathbf{t}_{1y}(r, 0)$  or  $\mathbf{t}_{2y}(r, 0)$  (here 1 and 2 represent upper and lower materials, respectively):

$$\mathbf{K} = \lim_{r \rightarrow 0} \sqrt{2\pi r} \mathbf{t}_{1y}(r, 0) = \lim_{r \rightarrow 0} \sqrt{2\pi r} \mathbf{t}_{2y}(r, 0). \quad (44)$$

Equation (43) is expressed in the Cartesian coordinate systems, as follows:

$$\mathbf{K} = \lim_{z \rightarrow a} \sqrt{2\pi(z-a)} \mathbf{t}_{1y}(z). \quad (45)$$

**4.2.1. Intensity Factor of the Right Semi-Infinite Plane Piezoelectric Bimaterial with Screw Dislocation.** Using equation (13), equation (45) can be expressed as

$$\mathbf{K}_2 = \lim_{z \rightarrow a} \sqrt{2\pi(z-a)} \mathbf{t}_{1y}(z)$$

$$= \frac{c_{44}^{(1)} \mathbf{b} a \sqrt{a\pi} (2\varepsilon_{11}^{(1)} + c_{44}^{(1)}) v + (1 + c_{12}) \varepsilon_{11}^{(1)}}{(h_1 + h_2) 2c_{12} v + c_{44}^{(1)} v (1 + c_{12})}$$

$$\text{Re} \frac{1}{\sqrt{\left[1 + ie^{\pi i} (h_1+h_2) (z-(h_1-h_2)/2)i / (1 - ie^{\pi i} (h_1+h_2) (z-(h_1-h_2)/2)i)\right]^4 - a^2} - \sqrt{\left[1 + ie^{\pi i} (h_1+h_2) (\bar{z}_0-(h_1-h_2)/2)i / (1 - ie^{\pi i} (h_1+h_2) (\bar{z}_0-(h_1-h_2)/2)i)\right]^4 - a^2}}, \quad (48)$$

$$\mathbf{K}_1 = \lim_{z \rightarrow a} \sqrt{2\pi(z-a)} \mathbf{t}_{1y}(z)$$

$$= \sqrt{\frac{a}{4\pi}} c_{44}^{(1)} \mathbf{b} \frac{(2\varepsilon_{11}^{(1)} + c_{44}^{(1)}) v + (1 + c_{12}) \varepsilon_{11}^{(1)}}{2c_{12} v + c_{44}^{(1)} v (1 + c_{12})} \quad (46)$$

$$\cdot \text{Re} \frac{1}{\sqrt{z_0^2 - a^2} - \sqrt{\bar{z}_0^2 - a^2}},$$

where

$$c_{12} = \frac{c_{44}^{(1)}}{c_{44}^{(2)}}, \quad (47)$$

$$v = \frac{\varepsilon_{11}^{(1)}}{e_{15}^{(1)2}}.$$

**4.2.2. Intensity Factor of the Fine-Grained Piezoelectric Coating/Substrate with Edge Interfacial Crack and Screw Dislocation.** According to the above discussion, substituting equation (15) into equation (46), the intensity factor can be expressed as



where

$$c_{12} = \frac{c_{44}^{(1)}}{c_{44}^{(2)}}, \quad (49)$$

$$\nu = \frac{\varepsilon_{11}^{(1)}}{e_{15}^{(1)2}}.$$

## 5. Numerical Process and Results

This section is divided into two parts. Firstly, some numerical applications to verify the obtained solutions are given, in the case when we reduce the current cases to simpler one (as shown in Figure 3(b)). Then, the influence of material constants, crack length, coating thickness on the image force, and intensity factor is studied.

*5.1. Study of a Screw Dislocation in Two Bonded Piezoelectric Right Semi-Infinite Planes as Shown in Figure 3(b).* As shown in Figure 3(b), by equations (23) and (24), based on the previous discussion, we got the image force acting on the dislocation near a traction-free and a charge-free boundary as

$$F_x - iF_y = \frac{\mathbf{b}\mathbf{b}^T}{2\pi} \mathbf{L}^{(1)} \left[ \frac{1}{\xi_0 + \bar{\xi}_0} + \mathbf{G} \left( \frac{1}{\xi_0 - \bar{\xi}_0} - \frac{1}{\xi_0 + \xi_0} \right) \right]. \quad (50)$$

When the material parameters of upper and lower materials are same, i.e.,  $\mathbf{L}^{(1)} = \mathbf{L}^{(2)}$ , we obtained

$$F_x = \text{Re}(F_x - iF_y) = \text{Re} \left\{ \frac{\mathbf{b}\mathbf{b}^T}{2\pi} \mathbf{L}^{(1)} \left[ \frac{1}{\xi_0 + \bar{\xi}_0} + \mathbf{G} \left( \frac{1}{\xi_0 - \bar{\xi}_0} - \frac{1}{\xi_0 + \xi_0} \right) \right] \right\}$$

$$= -\frac{\mathbf{b}\mathbf{b}^T \mathbf{L}^{(1)}}{2\pi} \frac{1}{\xi_0 + \bar{\xi}_0}, \quad (51)$$

$$F_y = \text{Im}(F_x - iF_y) = \text{Im} \left\{ \frac{\mathbf{b}\mathbf{b}^T}{2\pi} \mathbf{L}^{(1)} \left[ -\frac{1}{\xi_0 + \bar{\xi}_0} + \mathbf{G} \left( \frac{1}{\xi_0 - \bar{\xi}_0} - \frac{1}{\xi_0 + \xi_0} \right) \right] \right\} = 0.$$

The above results agree with the ones given by Pak [5], Liu et al. [6], and Chen et al. [18].

The strength of piezoelectricity is characterized by the electric-mechanical coupling factor  $k = \sqrt{(e_{15}^2)/(c_{44}\varepsilon_{11})}$ . As shown in Figure 3(d), we choose the PZT-6B ceramic and the PZT-5H ceramic as material 1, respectively. The ceramic's properties are given by Chen et al. [18] as follows:  $c_{44}^{(1)} = 2.71 \times 10^{10} \text{ N/m}^2$ ,  $e_{15}^{(1)} = 4.6 \text{ C/m}^2$ ,  $\varepsilon_{11}^{(1)} = 3.6 \times 10^{-9} \text{ C/Vm}$ ,  $k = 0.271$ ,  $c_{44}^{(1)} = 3.53 \times 10^{10} \text{ N/m}^2$ ,  $e_{15}^{(1)} = 17.0 \text{ C/m}^2$ ,  $\varepsilon_{11}^{(1)} = 1.51 \times 10^{-8} \text{ C/Vm}$ , and  $k = 0.542$ .

The force on the dislocation is normalized by

$$F_{*1} = \frac{b_z^2}{4\pi r_0}, \quad (52)$$

$$F_{*2} = \frac{b_\varphi^2}{4\pi r_0}.$$

The normalized force on the dislocation along  $x$ -axis versus angular position  $\theta$  (in degree) is shown in Figures 6 and 7.

It is observed that the force on the dislocation along the  $x$ -axis decreases with the increasing angle  $\theta$ . It means

the electric-free surface always attracts the dislocation. This conclusion agree with the ones given by Chen et al. [18].

*5.2. Study of the Interactions of the Dislocation with the Fine-Grained Piezoelectric Coating/Substrate Structure as Shown in Figure 1.* It is known from the characteristics of fine-grained piezoelectric materials that the piezoelectric and dielectric constants of the material reach the level of the large-grained piezoelectric material, and that the elastic modulus is much larger than that of the large-grained piezoelectric material. Therefore, in the following discussion, we assume that the piezoelectric coating/substrate has the same piezoelectric and dielectric constants.

In this part, some numerical applications were firstly considered to be presented. When we have a screw dislocation loading in a semi-infinite plane with an edge interface crack, the lower half of the plane, we choose the PZT-5H ceramic, and in the lower half plane, suitable piezoelectric materials can be selected. The PZT-5H ceramic's properties are given by Pak [1]:  $c_{44}^{(2)} = 3.53 \times 10^{10} \text{ N/m}^2$ ,  $e_{15}^{(2)} = 17.0 \text{ C/m}^2$ , and  $\varepsilon_{11}^{(2)} = 1.51 \times 10^{-8} \text{ C/Vm}$ .

Assume that  $h_2/h_1 = 100$ ,  $r_0/h_1 = 0.1$ , and  $\mathbf{b} = [b_z, 0]$ .

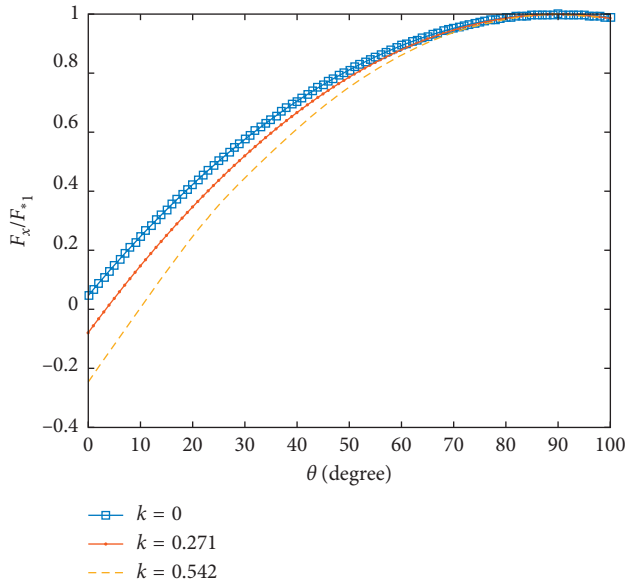


FIGURE 6: Force on the dislocation  $b_z$  along the  $x$ -axis versus angular position  $\theta$ .

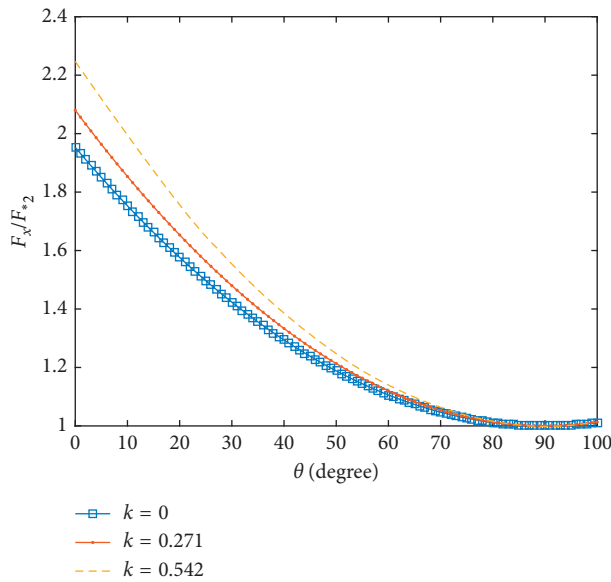


FIGURE 7: Force on the dislocation  $b_\varphi$  along the  $x$ -axis versus angular position  $\theta$ .

5.2.1. Study of the Influence of the Parameter  $c_{44}^{(1)}/c_{44}^{(2)}$ . Relationship between different image forces and angle  $\theta$  for different values of the parameter  $c_{44}^{(1)}/c_{44}^{(2)}$  is discussed in this section.

5.2.2. Study of the Influence of the Crack Length. Relationship between different image forces and angle  $\theta$  for different values of the crack length  $a$  is discussed in this section.

5.2.3. Study of the Influence of Parameter  $h_1$ . Relationship between different image forces and angle  $\theta$  for different values of the parameter  $h_1$  is discussed in this section.

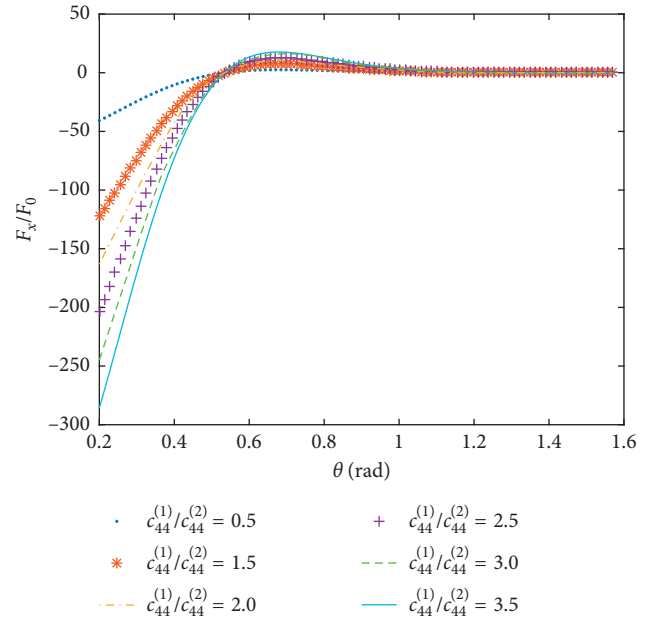


FIGURE 8: Relationship between image force  $F_x$  and angle  $\theta$  for different values of the parameter  $c_{44}^{(1)}/c_{44}^{(2)}$ .

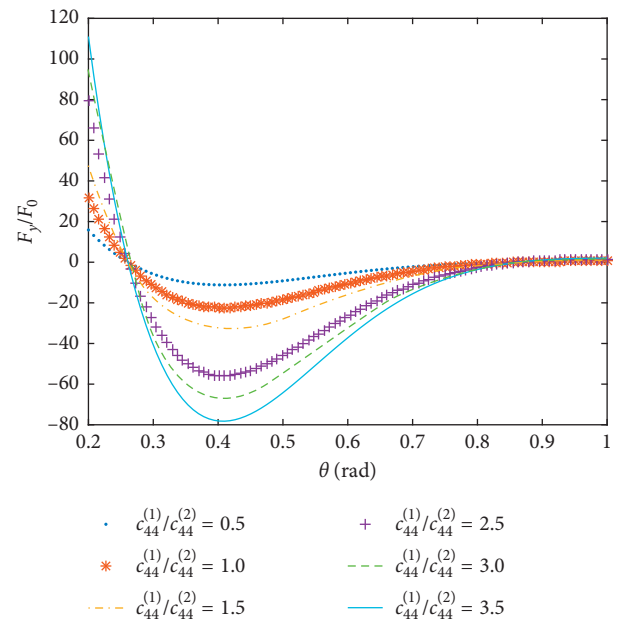


FIGURE 9: Relationship between image force  $F_y$  and angle  $\theta$  for different values of the parameter  $c_{44}^{(1)}/c_{44}^{(2)}$ .

5.3. Discussion of Results. Figures 8 and 9 show the changes of the image force  $F_x$  and  $F_y$ , respectively, with angle  $\theta$  when the elastic modulus changes. It can be seen from the figures that the elastic modulus has a significant effect on the image force, and the image force near the interface is the largest ( $0.2 < \theta < 0.6$ ). However, when the  $\theta$  increases to a certain value ( $\theta > 0.6$ ), the influence of the elastic modulus on the image force is very small, which is caused by the shielding effect of the crack on the dislocation (where  $a = 1$  mm,  $h_1 = 1$  mm, and  $F_0 = (b_z^2)/(h_1 + h_2)$ ).

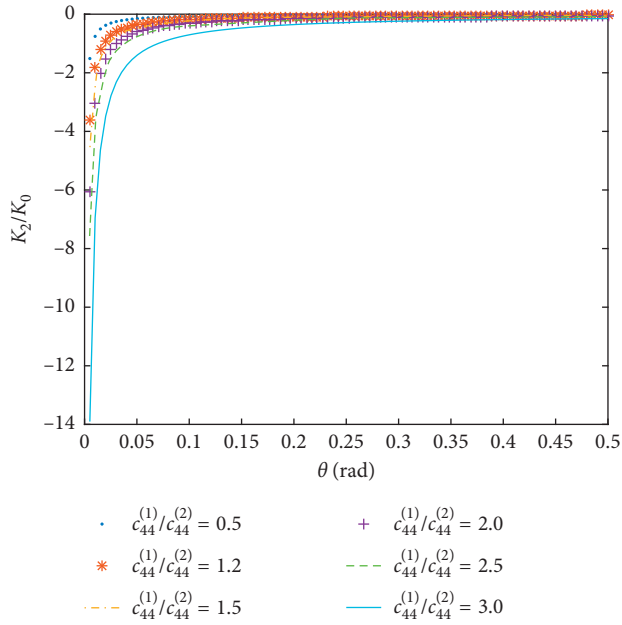


FIGURE 10: Relationship between IFs  $K_2$  and angle  $\theta$  for different values of the parameter  $c_{44}^{(1)}/c_{44}^{(2)}$ .

It can be seen in Figure 10 that the intensity factor  $K_2$  decreases with increase in elastic modulus and the intensity factor is negative, indicating that the dislocation plays a shielding effect on the crack. In addition, when the angle  $\theta$  is greater than 0.25, the change of the elastic modulus has little effect on the intensity factor (where  $a = 1$  mm,  $h_1 = 1$  mm, and  $F_0 = (b_z^2)/(h_1 + h_2)$ ).

In Figures 11 and 12, the law of variation of  $F_x$  and  $F_y$  with angle  $\theta$  is given when the crack length has different values. When  $a = 1$  mm, the influence of  $\theta$  on the image force is very small. With the change of crack length, the image force is greatly influenced by  $\theta$ . However, the image force gradually tends to be balanced with the increase in angle  $\theta$ , as in previous studies (where  $c_{44}^{(1)}/c_{44}^{(2)} = 1.2$ ,  $h_1 = 1$  mm, and  $F_0 = (b_z^2)/(h_1 + h_2)$ ).

In Figure 13, it can be seen that the crack length has a great influence on the intensity factor  $K_2$ . With the increasing crack length, the strength factor first increases and then decreases, and the dislocation near the crack is a maximum. This indicates that the dislocation can not only delay the crack growth but it can also promote it. However, the intensity factor tends to be balanced with the increasing angle  $\theta$ , when the dislocation is far away from the crack, at which point it has little effect on the intensity factor (where  $c_{44}^{(1)}/c_{44}^{(2)} = 1.2$ ,  $h_1 = 1$  mm, and  $F_0 = (b_z^2)/(h_1 + h_2)$ ).

Figures 14 and 15 show that the coating thickness has a great influence on the image force  $F_x$  and  $F_y$ , respectively, and decreases with the increasing coating thickness. The maximum value of the image force is near the crack, indicating that the dislocation can affect the crack. However, with the increasing angle  $\theta$ , the influence of coating thickness on image force gradually decreases. When the angle  $\theta$  is greater than 0.8, the coating thickness has almost

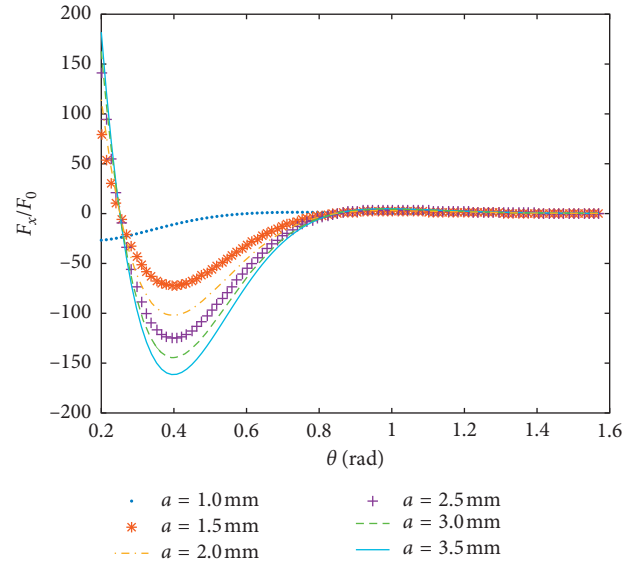


FIGURE 11: Relationship between image force  $F_x$  and angle  $\theta$  for different values of the crack length  $a$ .

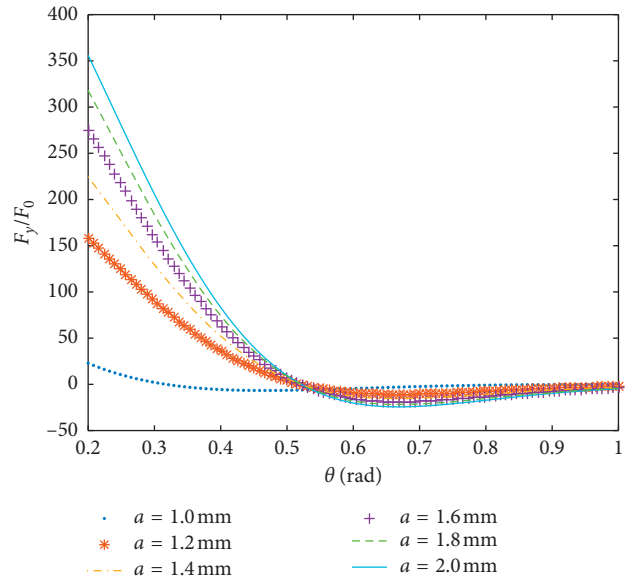


FIGURE 12: Relationship between image force  $F_y$  and angle  $\theta$  for different values of the crack length  $a$ .

no effect on image force (where  $c_{44}^{(1)}/c_{44}^{(2)} = 1.2$ ,  $a = 1$  mm, and  $F_0 = (b_z^2)/(h_1 + h_2)$ ).

Figure 16 shows that the intensity factor  $K_2$  decreases with the increasing coating thickness and the maximum of the intensity factor at the dislocations near the interface and the strength factor gradually tends to be stable with the increasing angle  $\theta$  also indicating that dislocation near a crack can prevent crack growth (where  $c_{44}^{(1)}/c_{44}^{(2)} = 1.2$ ,  $a = 1$  mm, and  $K_0 = ((a\sqrt{a\pi})/(2(h_1 + h_2)))c_{44}^{(1)}b_z$ ).

Finally, it can be concluded that the elastic modulus of the material and the coating thickness plays an important role in fracture mechanics for the fine-grained piezoelectric coating/substrate structure.

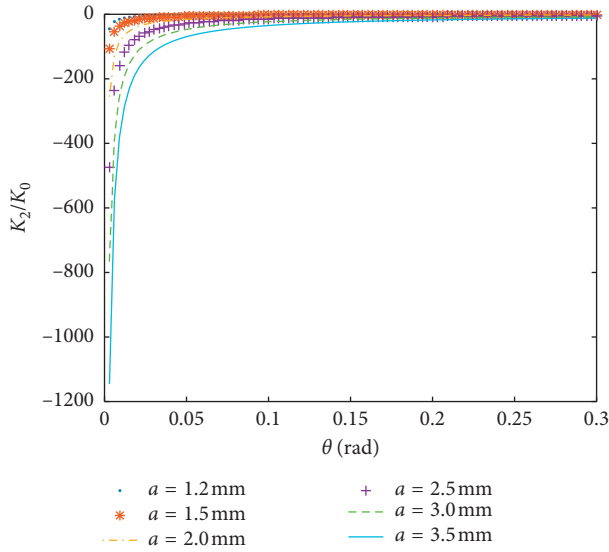


FIGURE 13: Relationship between IFs  $K_2$  and angle  $\theta$  for different values of the crack length  $a$ .

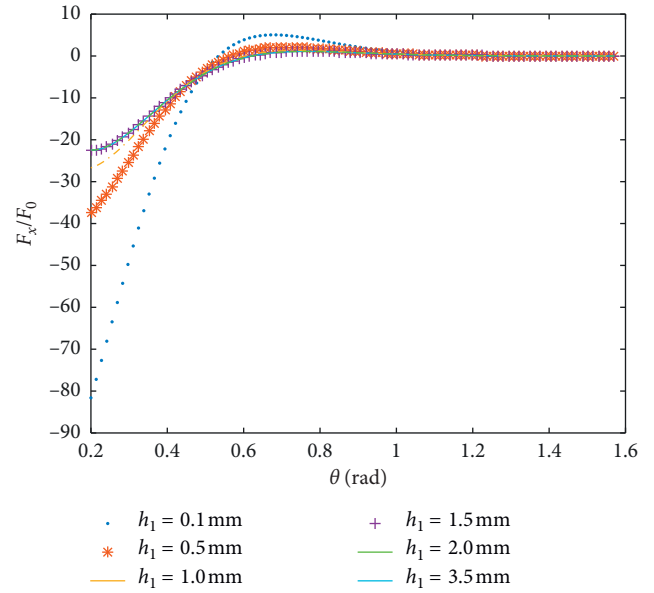


FIGURE 15: Relationship between image force  $F_x$  and angle  $\theta$  for different values of parameter  $h_1$ .

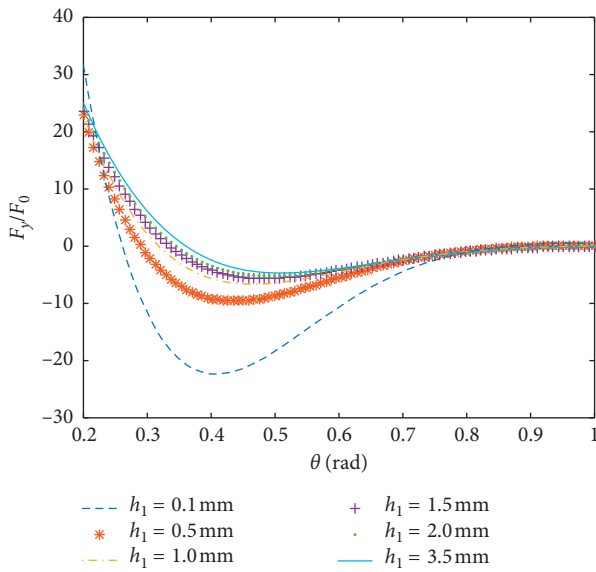


FIGURE 14: Relationship between image force  $F_y$  and angle  $\theta$  for different values of parameter  $h_1$ .

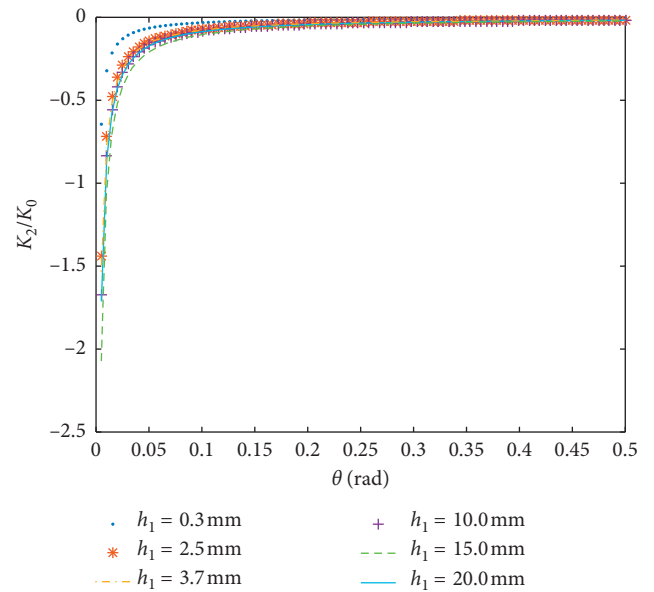


FIGURE 16: Relationship between IFs  $K_2$  and angle  $\theta$  for different values of parameter  $h_1$ .

### 6. Conclusions

The interaction between micro- and macroscopic crack (i.e., Griffith-type interface cracks and screw dislocation) in fine-grained piezoelectric coating/substrate was considered in this paper. The mapping function method is utilized to transform the complex geometric model into a relatively simple model, and the image force, intensity factor of the right semi-infinite piezoelectric bimaterials with the edge interfacial crack, and the finite thickness coating/substrate structure with the screw dislocation are obtained. Based on the solutions for these two problems, the relationship between microscopic defects and

macroscopic cracks in the fine-grained piezoelectric coating/substrate is provided.

A numerical application was used to analyze the case of the screw dislocation and the edge interfacial crack in a finite thickness coating/substrate, and the results show that the coating thickness, elastic modulus, and the length of the crack have a significant influence on the dislocation and interface crack. The numerical results also show that, to better resist fracture, it is necessary to choose a coating material with a larger elastic modulus and smaller thickness to realize better resistance to fracturing of the coating/

substrate structure. These characteristics reflect the superior properties of fine-grained piezoelectric coating materials.

## Appendix

The mapping function  $\zeta = f(z) = -i[(1 + ie^{\pi/(h_1+h_2)}(z - ((h_1 - h_2)/2)i)/(1 - ie^{\pi/(h_1+h_2)}(z - ((h_1 - h_2)/2)i))]^2$  can be decomposed into the following mapping functions (Figures 4 and 5).

In Figure 4,  $z_1 = z - ((h_1 - h_2)/2)i$ ,  $z_2 = (\pi/(h_1 + h_2))z_1$ ,  $z_3 = -z_2$ ,  $z_4 = e^{z_3}$ ,  $z_5 = iz_4$ ,  $z_6 = ((1 + z_5)/(1 - z_5))^2$ , and  $\zeta = -iz_6$ .

The mapping function  $\xi = \sqrt{\zeta^2 - a^2}$  can be decomposed into the following mapping functions (Figure 16).

In Figure 5,  $\xi = \sqrt{\zeta^2 - a^2}$ .

## Data Availability

All the numerical calculated data used to support the findings of this study can be obtained by calculating the equations in the paper, and piezoelectric material parameters are taken from reference [1]. The codes used in this paper are available from the corresponding author upon request.

## Conflicts of Interest

The authors declare that there are no conflicts of interest regarding the publication of this paper.

## Acknowledgments

This study was funded by the National Natural Science Foundation of China (11972019 and 11802194) and the Doctoral Scientific Research Foundation (20182051).

## References

- [1] Y. E. Pak, "Crack extension force in a piezoelectric material," *Journal of Applied Mechanics*, vol. 57, no. 3, pp. 647–653, 1990.
- [2] P. Y. Zhang and P. Tong, "Fracture mechanics for a mode III crack in a piezoelectric material," *International Journal of Solids and Structures*, vol. 33, no. 3, pp. 343–359, 1996.
- [3] X. F. Li and K. Y. Lee, "Electroelastic behavior of a rectangular piezoelectric ceramic with an anti-plane shear crack at arbitrary position," *European Journal of Mechanics—A/Solids*, vol. 23, no. 4, pp. 645–658, 2004.
- [4] B. Chen, Z. M. Xiao, and K. M. Liew, "A screw dislocation interacting with a finite crack in a piezoelectric medium," *International Journal of Engineering Sciences*, vol. 42, no. 13–14, pp. 1325–1345, 2004.
- [5] Y. E. Pak, "Force on a piezoelectric screw dislocation," *Journal of Applied Mechanics*, vol. 57, no. 4, pp. 863–869, 1990.
- [6] J. X. Liu, S. Y. Du, and B. Wang, "A screw dislocation interacting with a piezoelectric bimaterial interface," *Mechanics Research Communications*, vol. 26, no. 4, pp. 415–420, 1999.
- [7] B. Jin and Q. H. Fang, "Piezoelectric screw dislocations interacting with a circular inclusion with imperfect interface," *Archive of Applied Mechanics*, vol. 78, no. 2, pp. 105–116, 2008.
- [8] X. Wang and Y. Xu, "Interaction between a piezoelectric screw dislocation and a finite crack with surface piezoelectricity," *Zeitschrift Ffur Angewandte Mathematik und Physik*, vol. 66, no. 6, pp. 3679–3697, 2015.
- [9] R. Bagheri, M. Ayatollahi, and S. M. Mousavi, "Analysis of cracked piezoelectric layer with imperfect non-homogeneous orthotropic coating," *International Journal of Mechanical Sciences*, vol. 93, pp. 93–101, 2015.
- [10] Y. B. Zhang, Q. H. Fang, and Y. W. Liu, "The interaction between a screw dislocation and a nano-inhomogeneity with a semi-infinite wedge crack penetrating the interface," *Acta Mechanica*, vol. 225, no. 2, pp. 581–594, 2014.
- [11] M. H. Shen and S. Y. Hung, "Screw dislocation near a piezoelectric oblique edge crack," *Meccanica*, vol. 51, no. 6, pp. 1445–1456, 2016.
- [12] Y. W. Liu, C. Xie, M. Deng, Q. H. Fang, and B. Jin, "Screw dislocations and an interfacial blunt crack with viscoelastic interface," *Theoretical and Applied Fracture Mechanics*, vol. 52, no. 3, pp. 146–153, 2009.
- [13] M. Fan, D. K. Yi, and Z. M. Xiao, "Elastic-plastic stress investigation for an arc-shaped interface crack in composite material," *International Journal of Mechanical Sciences*, vol. 83, pp. 104–111, 2014.
- [14] M. Fan, D. K. Yi, and Z. M. Xiao, "Elastic-plastic fracture behavior analysis on a griffith crack in the cylindrical three-phase composites with generalized irwin mode," *International Journal of Applied Mechanics*, vol. 6, no. 4, pp. 1450045–1450066, 2014.
- [15] C. J. Xiao, Z. X. Li, L. Y. Zhu, and H. T. Zhang, "Effect of grain size of BaTiO<sub>3</sub> ceramics on thermal expansion and electrical properties," *International Journal of Thermophysics*, vol. 35, no. 2, pp. 346–351, 2014.
- [16] X. X. Tian, S. Qu, H. Ma, Z. Pei, and B. Wang, "Effect of grain size on dielectric and piezoelectric properties of bismuth layerstructure CaBi<sub>2</sub>Nb<sub>2</sub>O<sub>9</sub> ceramics," *Journal of Materials Science: Materials in Electronics*, vol. 27, no. 12, pp. 13309–13313, 2016.
- [17] S. Yu, P. Yongping, C. Yongfei, and L. Yanjie, "Enhanced grain size effect on electrical characteristics of fine grained BaTiO<sub>3</sub> ceramics," *Journal of Materials Science: Materials in Electronics*, vol. 28, no. 17, pp. 13229–13235, 2017.
- [18] B. J. Chen, Z. M. Xiao, and K. M. Liew, "A screw dislocation in a piezoelectric bi-material wedge," *International Journal of Engineering Sciences*, vol. 40, no. 15, pp. 1665–1685, 2002.



